Relative Permittivity of Dimethylsulfoxide and *N*,*N*-Dimethylformamide at Temperatures from (278 to 328) K and Pressures from (0.1 to 5) MPa†

Johannes Hunger and Richard Buchner

Institut für Physikalische und Theoretische Chemie, Universität Regensburg, D-93040 Regensburg, Germany

Mohamed E. Kandil, Eric F. May, and Kenneth N. Marsh*

Centre for Energy, School of Mechanical Engineering, The University of Western Australia, Crawley W.A. 6009, Australia

Glenn Hefter

Chemistry Department, Murdoch University, Murdoch, W.A. 6150, Australia

Relative permittivities (ε_r) have been measured at two frequencies with an expanded ($k = 2$) uncertainty of 0.1 using a re-entrant radio frequency resonator in the pressure range (0.1 to 5) MPa at temperatures from (278 to 328) K for *N*,*N*-dimethylformamide (DMF) and (293 to 328) K for dimethylsulfoxide (DMSO). At 298.15 K and 0.1 MPa, the assessed literature averages of 38.4 ± 1.8 and 47.3 ± 1.8 for DMF and DMSO, respectively, are consistent with the values of 37.2 ± 0.1 and 46.0 ± 0.1 determined in this work. Possible sources of uncertainty are discussed. An empirical description of $\varepsilon_r(p,T)$ is given that can be used to calculate the temperature and pressure derivatives of ε_r. Kirkwood *g* factors calculated using the present data show only minimal dipole−dipole correlations for both DMF and DMSO.

Introduction

Accurate values of the pressure and temperature dependence of relative permittivities (dielectric constants), ε_r, are of scientific and industrial interest, since they are required for the application of various theories and for reliable process simulation. For example, the pressure dependence of ε_r needs to be known to model the compression of a solvent by the electric field of an ion via the Drude−Nernst equation[1] or to apply the Debye−Hückel limiting law to the volumetric properties of electrolyte solutions.[2] Similar requirements exist for the first and second temperature derivatives of ε_r for modeling enthalpies of solution and heat capacities.

However, reliable studies of $\varepsilon_r(p,T)$ of molecular solvents in the literature are scarce,[3] with most of the available experimental data, particularly for solvents suited to electrolyte studies, focused on $(\partial\varepsilon_r/\partial T)_p$, often obtained over very limited temperature ranges. In this work $\varepsilon_r(p,T)$ has been measured for *N*,*N*-dimethylformamide (DMF) and dimethylsulfoxide (DMSO), with a particular focus on $(\partial\varepsilon_r/\partial p)_T$. Both of these solvents are widely used in separation processes because they dissolve a very diverse range of organic and inorganic compounds: DMF is used on a large scale as a solvent for polymers and paints, while DMSO has pharmaceutical applications.[4] Reliable data for $\varepsilon_r(p,T)$ of DMF and DMSO will improve the fundamental models used to describe them, which may in turn lead to better predictions of their thermophysical properties by simulation packages used to design new industrial processes based on these solvents.

The experimental methods available to determine relative permittivity over a range of temperatures and pressures have been summarized recently.[5] One method well-suited to $\varepsilon_r(p,T)$ measurements of fluids utilizes robust re-entrant cavity resonators. Measurements of $\varepsilon_r(p,T)$ with such instruments have been used to determine high-pressure phase boundaries and liquid volume fractions in binary[6−8] and multicomponent hydrocarbon mixtures.[9,10] Re-entrant resonators have also been used for accurate measurements of molar polarizability and/or permittivity and dipole moments in nonpolar fluids and mixtures,[11,12] weakly polar pure fluids[13] and strongly polar water.[14−16] In the present study a three-lobed re-entrant radio frequency resonator was used to determine the generalized complex permittivity, $\hat{\eta}(p,T)$, over the pressure range (0.1 to 5) MPa at temperatures from (278 to 328) K for DMF and (293 to 328) K for DMSO. The generalized complex permittivity, $\hat{\eta} = \varepsilon_r - i\eta''$, where $i = (-1)^{1/2}$ and $\eta'' = \varepsilon'' + \kappa/2\pi f\varepsilon_0$, comprises the relative permittivity, ε_r, the total loss, η'', the dielectric loss, ε'', and the Ohmic loss, which is determined by the electrical conductivity, κ, the frequency of the electromagnetic radiation, *f*, and the electric constant, $\varepsilon_0 = 8.854\,187\,817... \cdot 10^{-12}$ F·m^{-1}.[17]

The temperature dependence of ε_r for these two solvents has been studied frequently (see Supporting Information), although the results are not in very good agreement. To the best of our knowledge, apart from the data of Uosaki et al. (see later), for DMSO at 298.15 K, no such measurements have been made for the neat liquids at pressures above ambient.

Apparatus and Materials

Analytical grade DMSO (mass fraction $w > 0.999$) and DMF ($w > 0.998$) were obtained from Ajax Finechem (Australia) and

† Part of the "Josef M. G. Barthel Festschrift".

* To whom correspondence should be addressed. E-mail: ken.marsh@canterbury.ac.nz.

10.1021/je9010773
Published on Web 02/11/2010

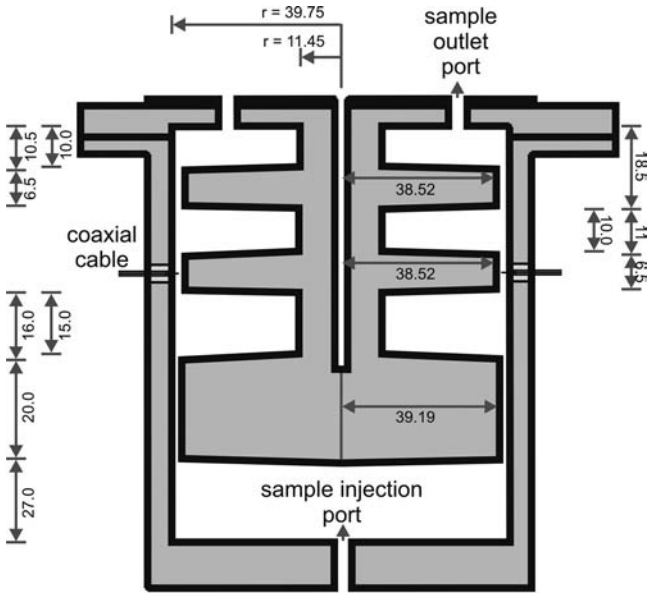

Figure 1. Schematic representation of the three-lobed cavity resonator. Key dimensions for the cavity are given in millimeters.

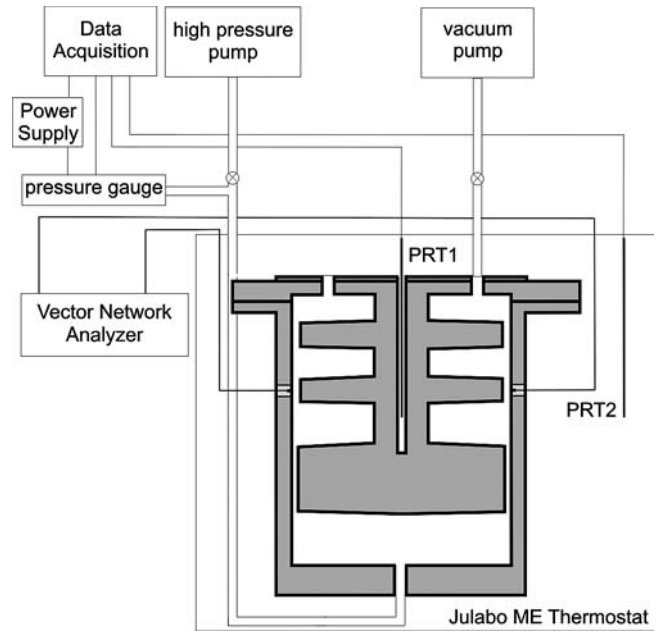

Figure 2. Schematic of the experimental system used for the measurements.

used without further purification. The water mass fraction, determined by coulometric Karl Fischer titration, was $4 \cdot 10^{-4}$ and $5.5 \cdot 10^{-4}$ for the DMSO and DMF samples, respectively. Approximate conductivities of DMF and DMSO were determined with a relative uncertainty of ± 10 %, with a four-terminal conductivity probe to be ($4 \cdot 10^{-4}$ and $1.3 \cdot 10^{-3}$) $S \cdot m^{-1}$, respectively, at approximately 297 K.

A schematic of the re-entrant cavity resonator is shown in Figure 1. This cavity had three "lobes" which resulted in three radio frequency modes, with vacuum resonance frequencies of approximately 170 MHz, 675 MHz, and 1.12 GHz. The relative deviations of these vacuum frequencies from those predicted with the nominal cavity dimensions using the extended waveguide model of Goodwin et al.[6] were −1.5 %, +1.0 %, and +7.8 %, respectively. Such deviations are typical of those reported elsewhere.[8] While the vacuum resonance frequencies depended sensitively on the cavity dimensions, the measured values of $\varepsilon_r(p,T) \cong (f(p,T)/f(0,T))^2$, being derived from frequency ratios, were insensitive to the cavity dimensions. The small effects of pressure and temperature on the vacuum resonance frequencies were accounted for by calibrating the resonator with helium as described in the next section.

The resonator was constructed from two type 316 stainless steel sections bolted together, with an indium O-ring providing a pressure seal and good electrical contact between the two sections. Unfortunately, the seal was not reliable at $p > 8$ MPa at temperatures above 328 K. The inner surfaces of the cavity that formed the boundaries for the radio frequency resonances were plated with gold to a thickness of 30 μm. This increased the quality factor of the resonances by decreasing the resistivity losses that occurred in the bounding conductor. High vacuum quality factors allow more reliable measurements of the imaginary part of $\hat{\eta}(p,T)$. Furthermore, the frequency dependence of the vacuum quality factor of the resonances is simpler to model if the boundary conductor is nonmagnetic.[15]

A schematic of the experimental setup used to make the measurements as a function of temperature and pressure is shown in Figure 2. The cavity resonator was placed in a Julabo ME thermostat filled with silicone oil M5 (Carl Roth, Germany), with a long-term temperature stability of ± 0.02 K. The temperatures of the bath and of the cavity were measured with

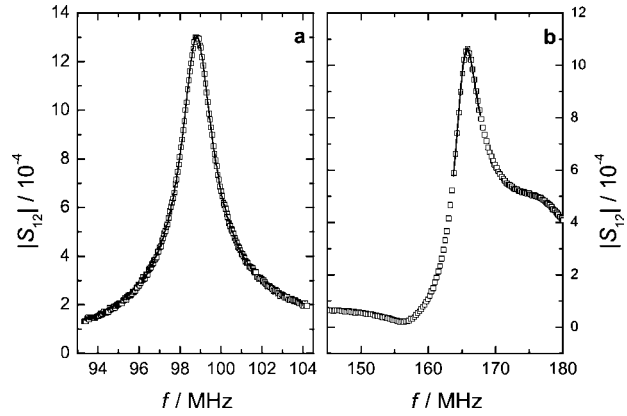

Figure 3. Magnitude of the complex scattering parameter, $|S_{12}|$, for: (a) mode 2 and (b) mode 3, for DMSO at $T \approx 293.15$ K and $p \approx 0.1$ MPa. Symbols represent measured values; line corresponds to fit with eq 1.

two 100 Ω platinum resistance thermometers (PTRs) connected to an Agilent 34970A data acquisition/switch unit using a four-wire configuration. The thermometer PRT1, used to measure the cavity temperature, was placed in the central well as shown in Figure 2. The two PRTs were calibrated against a 25 Ω standard PRT (Hart Scientific model 5681) with a standard uncertainty of ± 0.05 K. When the bath temperature was close to ambient, the agreement between the temperatures measured with the two PRTs was consistent with this uncertainty; however, at temperatures far from ambient, heat leaks into the resonator from elements located outside the bath resulted in differences of up to 0.2 K. The standard uncertainty in the temperature of the resonator was estimated to be ± 0.1 K.

Pressures within the cavity were monitored using a diaphragm strain-gauge type pressure transmitter (General Electric PTX 1400) with a full scale of 40 MPa. The transmitter was calibrated against a reference quartz crystal transducer (Paroscientific, model 1000, 7 MPa full scale) located outside the bath, which was isolated from the resonator during the measurements of DMF and DMSO. The relative uncertainty of the pressure

Table 1. Temperature, T, Pressure, p, and Resonance Frequencies, f_j, of Modes $j = 2$ and $j = 3$ for DMF[a]

T	p	f_2			f_3		
K	kPa	MHz	ε_{r2}	η''_2	MHz	ε_{r3}	η''_3
277.74	110	105.248	41.138	0.404	176.165	41.128	0.608
277.74	5088	105.241	41.279	0.410	176.013	41.267	0.620
277.73	2589	105.240	41.211	0.407	176.083	41.200	0.614
277.72	111	105.246	41.140	0.404	176.161	41.130	0.608
277.72	290	105.244	41.146	0.404	176.153	41.136	0.608
277.73	589	105.245	41.153	0.405	176.147	41.143	0.609
277.73	1088	105.244	41.168	0.405	176.131	41.157	0.610
277.73	2087	105.240	41.198	0.407	176.096	41.187	0.613
277.73	3086	105.238	41.227	0.408	176.064	41.216	0.615
277.73	4086	105.236	41.256	0.409	176.032	41.245	0.618
277.73	5086	105.240	41.279	0.410	176.012	41.268	0.620
277.73	2587	105.241	41.211	0.407	176.083	41.200	0.614
277.72	106	105.246	41.140	0.404	176.162	41.129	0.608
287.71	104	107.833	39.177	0.355	180.488	39.169	0.518
287.71	5081	107.815	39.318	0.360	180.317	39.309	0.528
287.74	2581	107.828	39.244	0.357	180.410	39.235	0.522
287.77	102	107.846	39.167	0.355	180.512	39.158	0.517
287.75	281	107.842	39.175	0.355	180.500	39.166	0.518
287.74	581	107.838	39.186	0.356	180.483	39.177	0.519
287.74	1080	107.834	39.201	0.356	180.463	39.192	0.520
287.74	2079	107.828	39.231	0.357	180.423	39.223	0.522
287.75	3081	107.826	39.259	0.358	180.389	39.251	0.524
287.75	4083	107.822	39.287	0.359	180.356	39.278	0.526
287.76	5087	107.827	39.309	0.360	180.336	39.300	0.527
287.75	2587	107.830	39.243	0.357	180.413	39.234	0.522
287.75	110	107.841	39.171	0.355	180.503	39.162	0.517
292.67	109	109.153	38.229	0.337	182.698	38.220	0.482
292.68	5084	109.126	38.373	0.341	182.511	38.363	0.491
292.68	2583	109.140	38.300	0.339	182.607	38.291	0.486
292.68	105	109.155	38.228	0.337	182.702	38.219	0.482
292.68	284	109.152	38.234	0.337	182.693	38.225	0.483
292.68	583	109.150	38.243	0.338	182.680	38.234	0.483
292.68	1083	109.146	38.258	0.338	182.660	38.249	0.484
292.68	2082	109.139	38.288	0.339	182.619	38.279	0.486
292.68	3081	109.135	38.317	0.340	182.582	38.307	0.488
292.68	4080	109.129	38.346	0.340	182.543	38.337	0.489
292.68	5080	109.125	38.373	0.341	182.510	38.363	0.491
292.68	2582	109.137	38.302	0.339	182.601	38.293	0.487
292.68	103	109.153	38.229	0.338	182.700	38.220	0.482
292.68	5081	109.126	38.373	0.341	182.511	38.363	0.492
292.68	2586	109.138	38.301	0.339	182.604	38.292	0.487
292.68	108	109.154	38.228	0.338	182.701	38.219	0.483
297.68	109	110.472	37.315	0.323	184.906	37.307	0.450
297.69	288	110.471	37.320	0.323	184.898	37.312	0.450
297.69	588	110.467	37.330	0.323	184.882	37.322	0.451
297.68	1088	110.459	37.348	0.324	184.855	37.340	0.452
297.69	2089	110.454	37.376	0.324	184.816	37.368	0.453
297.71	3089	110.453	37.401	0.325	184.785	37.393	0.454
297.72	4089	110.447	37.430	0.325	184.744	37.422	0.456
297.72	5090	110.442	37.458	0.326	184.707	37.450	0.457
297.72	3090	110.455	37.400	0.325	184.788	37.392	0.454
297.71	1091	110.470	37.341	0.324	184.872	37.333	0.451
297.71	112	110.475	37.313	0.323	184.909	37.306	0.450
302.73	101	111.734	36.471	0.301	187.016	36.464	0.417
302.73	5078	111.707	36.608	0.304	186.820	36.601	0.424
302.73	2579	111.711	36.545	0.302	186.905	36.537	0.420
303.11	101	111.818	36.415	0.300	187.158	36.408	0.415
303.11	281	111.816	36.421	0.300	187.148	36.414	0.415
303.12	581	111.818	36.427	0.300	187.142	36.420	0.416
303.11	1082	111.810	36.444	0.300	187.113	36.437	0.416
303.12	2085	111.805	36.472	0.301	187.075	36.465	0.418
303.13	3088	111.797	36.501	0.301	187.031	36.494	0.419
303.13	4088	111.790	36.529	0.302	186.990	36.522	0.420
303.13	5088	111.797	36.549	0.302	186.969	36.543	0.422
303.12	2589	111.800	36.487	0.301	187.052	36.480	0.418
303.12	112	111.821	36.414	0.300	187.162	36.406	0.414
307.72	111	113.056	35.617	0.290	189.229	35.610	0.392
307.71	5089	113.016	35.759	0.292	189.011	35.752	0.399
307.71	2589	113.028	35.693	0.291	189.109	35.685	0.396
307.72	111	113.055	35.618	0.289	189.230	35.610	0.392
307.73	290	113.055	35.622	0.289	189.224	35.614	0.392
307.73	588	113.050	35.632	0.290	189.206	35.624	0.393
307.74	1088	113.048	35.645	0.290	189.187	35.637	0.393
307.76	2086	113.040	35.673	0.290	189.144	35.666	0.395

Table 1. Continued

T / K	p / kPa	f_2 / MHz	ε_{r2}	η''_2	f_3 / MHz	ε_{r3}	η''_3
307.76	3085	113.031	35.702	0.290	189.098	35.695	0.396
307.74	4085	113.016	35.736	0.291	189.042	35.728	0.397
307.75	5084	113.024	35.754	0.291	189.023	35.747	0.399
307.72	2583	113.028	35.693	0.290	189.110	35.685	0.395
307.72	104	113.053	35.619	0.289	189.226	35.611	0.392
318.12	101	115.754	33.964	0.258	193.747	33.956	0.343
318.15	5079	115.723	34.094	0.261	193.531	34.089	0.348
318.14	2586	115.724	34.037	0.260	193.620	34.029	0.346
318.13	109	115.756	33.964	0.259	193.751	33.955	0.343
318.13	288	115.752	33.969	0.259	193.740	33.961	0.343
318.13	588	115.747	33.979	0.259	193.722	33.971	0.344
318.13	1088	115.740	33.995	0.260	193.694	33.986	0.344
318.12	2088	115.725	34.026	0.260	193.637	34.018	0.345
318.12	3088	115.711	34.056	0.261	193.582	34.048	0.346
318.12	4088	115.710	34.079	0.261	193.547	34.072	0.347
318.12	5088	115.714	34.099	0.265	193.517	34.094	0.350
318.12	2591	115.716	34.042	0.264	193.607	34.034	0.348
318.12	113	115.749	33.968	0.264	193.740	33.959	0.346
328.09	111	118.427	32.438	0.245	198.222	32.429	0.310
328.07	5087	118.362	32.580	0.246	197.947	32.574	0.314
328.07	2587	118.376	32.519	0.245	198.058	32.510	0.312
328.02	109	118.406	32.449	0.244	198.189	32.440	0.310
328.04	287	118.405	32.453	0.244	198.181	32.445	0.310
328.03	584	118.397	32.464	0.244	198.157	32.456	0.310
328.04	1084	118.389	32.479	0.244	198.127	32.471	0.310
328.05	2082	118.374	32.509	0.244	198.070	32.501	0.311
328.05	3081	118.355	32.541	0.244	198.004	32.533	0.312
328.04	4080	118.346	32.567	0.244	197.956	32.560	0.313
328.04	5079	118.349	32.587	0.244	197.923	32.582	0.313
328.05	2580	118.362	32.526	0.243	198.034	32.518	0.311
328.07	101	118.411	32.447	0.242	198.195	32.438	0.309

[a] ε_{rj} and η''_j are the real and imaginary parts of the generalized complex permittivity obtained with eq 2.

measurements made with the diaphragm strain-gauge transducer was ± 0.25 % of the reading, while the repeatability of the transducer was better than ± 1 kPa.

A computer-controlled high-pressure positive displacement pump (Quizix QX-6000, maximum pressure 40 MPa) was used to fill and then pressurize the solvent in the cavity. The filling process consisted of injecting about 240 cm^3 of liquid into the cavity, which had a total internal volume of 260 cm^3. A vacuum was then applied to the space above the liquid to degas the solvent. The remaining solvent volume was injected using the positive displacement pump, and once full, the pump was used to check for trapped gas bubbles by measuring the effective compressibility of the liquid. In all of the experiments reported, the apparent compressibility of the liquids, determined from the measured change in pressure corresponding to a known displaced volume, agreed with the expected value[18−20] within the experimental uncertainty.

The electromagnetic resonances of the re-entrant cavity were measured in transmission using a HP 8719ET vector network analyzer, with a frequency range of (0.05 to 13.5) GHz. The network analyzer recorded the complex scattering parameter $\hat{S}_{12}$ at 201 frequencies, centered on the approximate resonance frequency and spanning a range of approximately 10 times the resonance frequency. A typical sweep took about 50 s, and about 10 sweeps were averaged when obtaining the $\hat{S}_{12}$ used to determine the resonance parameters.

Method

Measurements of $\hat{\eta}(p,T)$ were made along isotherms. Following a change in bath temperature, approximately 3 h was required before the system was deemed to have achieved equilibrium, on the basis of the rates of change of the measured pressure, temperature, and resonance frequency. Following a change in pressure, approximately 0.8 h was required. The complex scattering parameters $\hat{S}_{12}$, measured once the system had equilibrated, were fit to the theoretical resonance function:[6]

$$\hat{S}_{12}(f) = \frac{\hat{A}f}{f^2 + (f_j + ig_j)^2} + \hat{B} \qquad (1)$$

Here f is the stimulus frequency, $\hat{A}$ and $\hat{B}$ are complex adjustable parameters, and $(f_j + ig_j)$ is the complex resonance frequency of mode j (= 1, 2, or 3). Nonlinear least-squares regression of $\hat{S}_{12}$ to eq 1 was used to determine the six parameters in the quantities $\hat{A}$, $\hat{B}$, and $(f_j + ig_j)$. Figure 3 shows values of $|\hat{S}_{12}|$ measured for the second and third modes with the cavity filled with DMSO at 293 K and 0.1 MPa. While mode 1 was measurable when the cavity was evacuated or filled with helium, the high permittivity of the target solvents meant that mode 1 was below the low-frequency limit of the network analyzer when the cavity was filled with either DMSO or DMF. When the cavity was filled with these solvents, the mode 2 resonance was located at approximately (95 to 120) MHz (Figure 3) and was isolated from other cavity resonances. In contrast, mode 3, which was located at approximately (165 to 200) MHz, was affected by interference from higher order modes. However, the interference did not seem to cause values of $\hat{\eta}(p,T)$ obtained from mode 3 to differ significantly from those obtained from mode 2, within the estimated experimental uncertainty. Accordingly, the real and imaginary parts of $\hat{\eta}(p,T)$ determined with both modes 2 and 3 are reported in Tables 1 and 2.

The complex total permittivity of each fluid was determined from the measured resonance frequencies, half-widths, and quality

Table 2. Temperature, T, Pressure, p, and Resonance Frequencies, f_j, of Modes $j = 2$ and $j = 3$ for DMSO[a]

T / K	p / kPa	f_2 / MHz	ε_{r2}	η''_2	f_3 / MHz	ε_{r3}	η''_3
292.85	110	98.751	46.701	0.564	165.344	46.655	0.895
292.85	5090	98.871	46.740	0.572	165.415	46.692	0.909
292.84	2591	98.810	46.721	0.568	165.378	46.674	0.902
292.85	113	98.752	46.700	0.565	165.344	46.654	0.895
292.84	293	98.755	46.702	0.565	165.345	46.657	0.895
292.85	592	98.762	46.705	0.565	165.348	46.660	0.896
292.84	1092	98.773	46.710	0.566	165.353	46.665	0.898
292.83	2091	98.795	46.720	0.568	165.364	46.674	0.901
292.84	3091	98.820	46.727	0.569	165.379	46.682	0.904
292.84	4091	98.844	46.735	0.571	165.394	46.689	0.907
292.84	5091	98.870	46.741	0.573	165.411	46.695	0.910
292.84	2591	98.810	46.721	0.568	165.374	46.676	0.902
292.84	112	98.751	46.701	0.565	165.341	46.656	0.895
297.86	111	99.426	46.062	0.523	166.462	46.024	0.816
297.86	5090	99.537	46.109	0.529	166.516	46.070	0.829
297.86	2590	99.479	46.087	0.526	166.484	46.050	0.823
297.85	111	99.422	46.065	0.523	166.453	46.028	0.816
297.86	291	99.425	46.068	0.523	166.453	46.031	0.817
297.86	591	99.431	46.071	0.523	166.455	46.035	0.818
297.86	1089	99.441	46.077	0.524	166.458	46.041	0.819
297.86	2089	99.464	46.086	0.525	166.469	46.050	0.821
297.86	3089	99.486	46.095	0.526	166.480	46.059	0.824
297.86	4089	99.509	46.104	0.528	166.492	46.068	0.826
297.86	5091	99.533	46.113	0.529	166.507	46.075	0.829
297.85	2591	99.475	46.091	0.526	166.474	46.055	0.823
297.86	114	99.419	46.068	0.523	166.446	46.032	0.816
302.77	112	100.089	45.446	0.489	167.566	45.412	0.750
302.78	5089	100.208	45.487	0.494	167.632	45.452	0.761
302.82	2589	100.154	45.461	0.491	167.607	45.428	0.755
302.84	111	100.103	45.433	0.489	167.587	45.401	0.749
302.84	291	100.107	45.435	0.489	167.588	45.403	0.750
302.85	591	100.114	45.438	0.489	167.592	45.406	0.750
302.84	1091	100.123	45.444	0.490	167.594	45.412	0.751
302.83	2090	100.143	45.456	0.491	167.600	45.424	0.754
302.63	3090	100.141	45.488	0.493	167.569	45.456	0.758
302.62	4091	100.163	45.498	0.495	167.580	45.466	0.760
302.62	5091	100.191	45.503	0.496	167.599	45.471	0.762
302.61	2591	100.129	45.484	0.493	167.561	45.453	0.757
302.6	101	100.072	45.461	0.489	167.532	45.431	0.751
307.85	111	100.868	44.739	0.457	168.902	44.690	0.690
307.85	5087	100.964	44.801	0.461	168.927	44.752	0.700
307.84	2587	100.911	44.774	0.459	168.905	44.726	0.694
307.84	109	100.859	44.747	0.457	168.884	44.700	0.690
307.85	288	100.862	44.750	0.457	168.883	44.703	0.690
307.85	587	100.866	44.755	0.457	168.882	44.708	0.691
307.85	1086	100.874	44.763	0.458	168.882	44.715	0.692
307.85	2086	100.894	44.775	0.459	168.888	44.727	0.693
307.84	3086	100.913	44.787	0.459	168.893	44.740	0.695
307.84	4086	100.934	44.797	0.460	168.902	44.750	0.696
307.85	5085	100.956	44.807	0.461	168.912	44.759	0.699
307.85	2584	100.906	44.778	0.459	168.894	44.731	0.694
307.84	107	100.854	44.751	0.457	168.873	44.705	0.689
317.75	116	102.326	43.459	0.411	171.296	43.436	0.599
317.75	5093	102.415	43.526	0.414	171.315	43.499	0.606
317.74	2595	102.366	43.496	0.413	171.299	43.470	0.602
317.73	117	102.320	43.464	0.411	171.289	43.439	0.599
317.74	296	102.325	43.466	0.411	171.292	43.440	0.599
317.77	595	102.332	43.468	0.411	171.298	43.442	0.600
317.75	1094	102.338	43.477	0.412	171.295	43.451	0.600
317.76	2093	102.357	43.490	0.412	171.299	43.463	0.602
317.78	3092	102.379	43.499	0.413	171.309	43.473	0.603
317.78	4092	102.396	43.513	0.414	171.312	43.486	0.605
317.78	5092	102.420	43.522	0.414	171.326	43.493	0.606
317.75	2592	102.367	43.495	0.413	171.304	43.468	0.603
317.73	113	102.318	43.466	0.412	171.289	43.439	0.599
327.57	99	103.885	42.150	0.376	173.884	42.138	0.528
327.57	5073	103.972	42.218	0.379	173.895	42.204	0.534
327.54	2573	103.918	42.193	0.378	173.874	42.179	0.532
327.54	95	103.877	42.157	0.377	173.874	42.143	0.529
327.55	274	103.881	42.159	0.378	173.876	42.145	0.529
327.56	572	103.885	42.164	0.378	173.875	42.150	0.530
327.57	1071	103.893	42.171	0.378	173.875	42.157	0.530
327.56	2070	103.907	42.187	0.378	173.873	42.172	0.531
327.56	3069	103.924	42.201	0.379	173.873	42.186	0.533

Table 2. Continued

T	p	f_2			f_3		
K	kPa	MHz	ε_{r2}	η''_2	MHz	ε_{r3}	η''_3
327.56	4068	103.940	42.216	0.380	173.874	42.200	0.534
327.57	5067	103.968	42.221	0.380	173.894	42.204	0.535
327.57	2569	103.916	42.194	0.379	173.876	42.177	0.532
327.57	91	103.877	42.157	0.379	173.878	42.141	0.529

[a] ε_j and η''_j are the real and imaginary parts of the generalized complex permittivity obtained with eq 2.

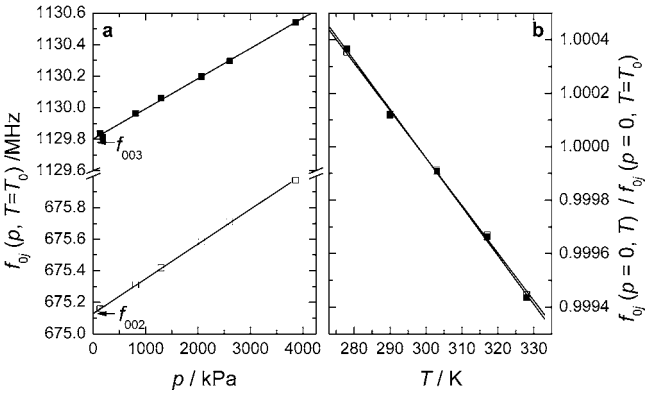

Figure 4. (a) Pressure calibration at $T_0 = 297.69$ K and (b) temperature calibration: □, mode 2; ■, mode 3 of the three-lobed reentrant cavity resonator. Lines represent linear regressions, and f_{0j} are the resonance frequencies corrected for the relative permittivity of He.

Table 3. Vacuum Resonance Frequencies f_{00j} at $T_0 = 297.69$ K, Measured Vacuum Half-Widths, g_{0j}, Pressure Coefficients, ϕ_j, and Temperature Coefficients, α_j, for Modes 2 and 3

	f_{00j}	g_{0j}	$10^7\ \phi_j$	$10^5\ \alpha_j$
j	MHz	MHz	kPa^{-1}	K^{-1}
2	675.128 ± 0.004	0.2063 ± 0.004	3.29 ± 0.03	−1.77 ± 0.04
3	1129.803 ± 0.008	0.2567 ± 0.008	1.68 ± 0.03	−1.83 ± 0.04

factors using the implicit model developed by Hamelin et al.[14] for the case of weak coupling to the measurement circuit.

$$\hat{\eta} = \left(\frac{f_{0j} + ig_{0j}}{f_j + ig_j}\right)^2 \frac{1 + (-1 + i)(f_j/f_{0j})^{3/2}\hat{\eta}/Q^0_{sj}}{1 + (-1 + i)/Q^0_{sj}} \qquad (2)$$

In eq 2 subscripts or superscripts "0" indicate properties of the vacuum resonance, and $Q^0_{sj} \equiv f_{0j}/2g_{0j}$ (≈ 2000) is the vacuum quality factor of mode j, determined by the effective resistivity of the bounding metal surface. The measured vacuum half-widths, g_{0j}, were about 2 to 10 times larger than expected on the basis of the literature electrical conductivity of gold.[21] This discrepancy can be attributed to the surface finish of the cavity's internal walls and is not critical to the measurements of $\hat{\eta}(p,T)$ because the values of $Q^0_{s,j}$ were stable. However, it was important to account for the changes in f_{0j} that occurred as the cavity temperature and fluid pressure were varied.

Helium Calibration. The relative permittivity of helium can be calculated as a function of temperature and pressure with an uncertainty smaller than the corresponding measurements of $\varepsilon_r(p,T)$.[22] Thus, resonance measurements when the cavity was filled with helium could be used to determine the effects of the cavity's thermal expansion and pressure dilation on the vacuum frequencies, thereby calibrating the resonator. For lossless fluids such as helium, with $\varepsilon_r \approx 1$, eq 2 simplifies to

$$\varepsilon_r(p,T) = \left(\frac{f_{0j} + ig_{0j}}{f_j + ig_j}\right)^2 \left(\frac{1 + (-1 + i)Q_j}{1 + (-1 + i)Q^0_{s,j}}\right) \qquad (3)$$

where Q_j is the mode's measured quality factor at a given (p,T). The vacuum resonance half-width is essentially independent of pressure and temperature, but the vacuum resonance frequency has the dependence

$$f_{0j} = f_{00j}(1 + \alpha_j(T - T_0) + \phi_j p) \qquad (4)$$

Here f_{00j} is the resonance frequency of mode j at $p = 0$ and an arbitrary reference temperature T_0, α_j is the effective temperature coefficient of the mode, and ϕ_j is the effective pressure coefficient of the mode. Measurements of $(f_j + ig_j)$ were made with the cavity filled with helium (mole fraction purity of 0.999999) at pressures ranging from (0.1 to 3.9) MPa at $T_0 = 297.69$ K and also at temperatures from (278 to 328) K at 2 MPa. At each condition, the value of $\varepsilon_r(p,T)$ for helium was calculated using the equation of state of McCarty and Arp[23] and the polarizability correlation of Harvey and Lemmon[24] as implemented in the software Refprop 8.0.[25] The calculated values of $\varepsilon_r(p,T)$ for helium were used in eq 3 to determine a value of f_{0j} at each pressure and temperature. The results of the pressure and temperature calibrations are shown in Figure 4. Linear least-squares regression of the data shown in Figure 4 was used to derive the parameters f_{00j}, α_j, and ϕ_j for each mode. The results for modes 2 and 3 are summarized in Table 3 and are comparable to those measured by other workers[8,11] with similar re-entrant cavities. The effective temperature coefficients of both modes are also in reasonable agreement with the coefficient of thermal expansion for stainless steel ($\alpha = 1.59 \cdot 10^{-5}\ K^{-1}$).[26] Also shown in Table 3 are the measured vacuum resonance half-widths that were used in eqs 2 and 3 for the analysis of all of the data obtained for helium, DMF, and DMSO.

Results and Discussion

Temperatures, pressures, frequencies, and the ε_r and $\hat{\eta}$ values obtained from the analysis with eq 2 are presented in Table 1 for DMF and Table 2 for DMSO, with pressures listed in temporal order. An analysis of the effects of uncertainties in the measured variables on the uncertainty in ε_r is given below.

Modeling. A least-squares regression of $\varepsilon_r(p,T)$ via the empirical eq 5 was used to determine the adjustable parameters A_1, A_2, B_1, B_2, and C_1

$$\varepsilon_r(p,T) = A_1 + A_2 p + (B_1 + B_2 p)T + C_1 T^2 \qquad (5)$$

The parameters B_2 (for DMF) and C_1 (for DMSO) were not statistically significant and thus were set equal to zero for DMF and DMSO, respectively. The other parameters, together with fit qualities, are summarized in Table 4. The derivatives

Table 4. Regression Parameters for the Three-Dimensional Fit of $\varepsilon_r(p,T)$ Using Equation 5 for Mode 2 for DMF and DMSO[a]

	A_1	$A_2 \cdot 10^6$ / kPa	B_1 / K	$B_2 \cdot 10^7$ / kPa·K	$C_1 \cdot 10^4$ / K^2	σ
DMF mode 2	141.31 ± 0.66	28.6 ± 1.0	–0.520 ± 0.004		5.75 ± 0.07	0.018
DMSO mode 2	85.13 ± 0.06	–43.8 ± 2.4	–0.1312 ± 0.0002	1.8 ± 0.8		0.014

[a] The standard error of the regression, σ, is also shown.

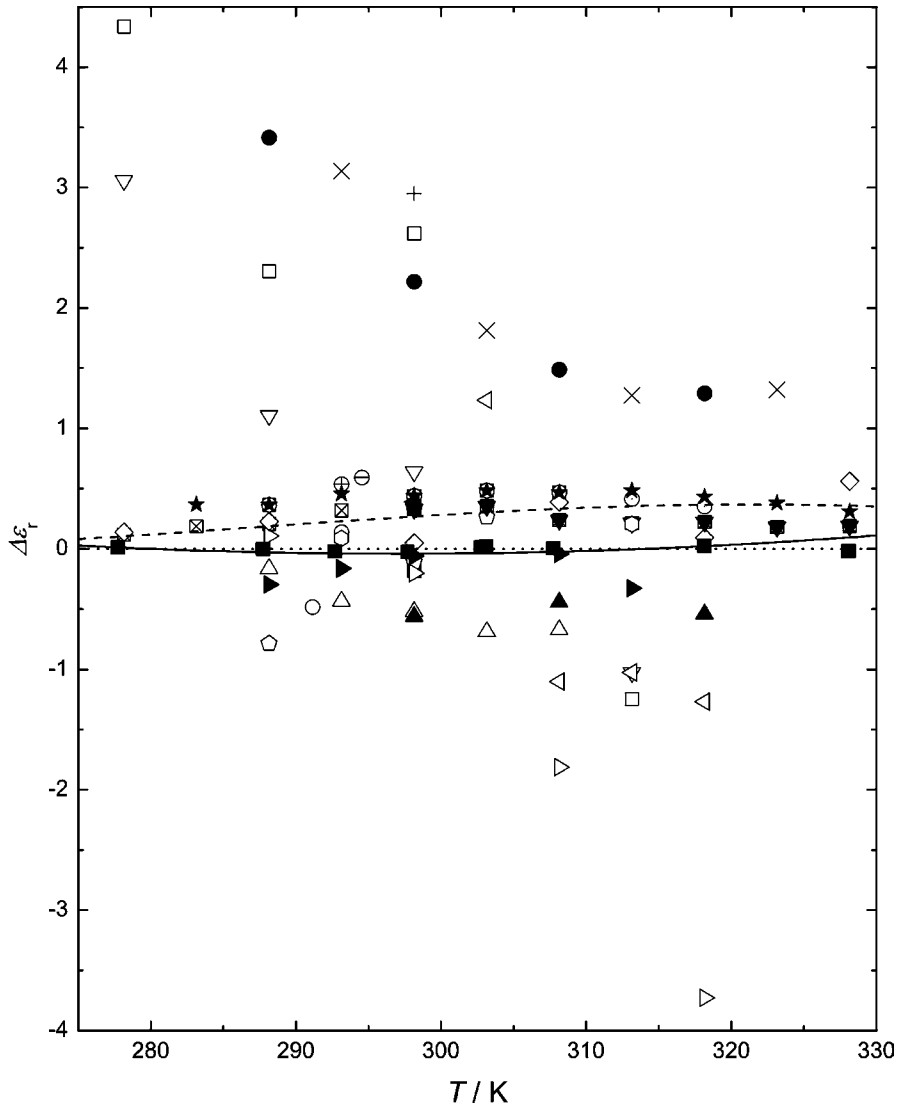

Figure 5. Absolute deviations, $\Delta\varepsilon_r = \varepsilon_{r,lit} - \varepsilon_r$, of literature data for DMF at $p = 101.3$ kPa MPa from permittivities, ε_r, calculated from eq 5 of this work using parameters obtained from mode 2: ■, measured values from this work; solid line represents $\varepsilon_r(T)$ recommended in ref 27; dashed line, recommended in ref 46. For details of the literature data see Supporting Information.

$(\partial\varepsilon_r/\partial T)_p$ and $(\partial\varepsilon_r/\partial p)_T$ are much smaller for DMSO than for DMF. For solvents of similar "character" (structure, molecular size, dipole moment, etc.) the magnitudes of $(\partial\varepsilon_r/\partial p)_T$ and $(\partial\varepsilon_r/\partial T)_p$ largely reflect changes in the dipole density (and hence the liquid density) with T and p. Consistent with this notion, both the isobaric expansivity, α_p, and the isothermal compressibility, κ_T, of DMF are larger than those of DMSO.[27] The small magnitude of the derivatives and the rather limited temperature range in the present study inevitably result in higher uncertainties in the parameters of eq 5 for DMSO compared with DMF (Table 4). It is notable that the pressure and temperature derivatives for both solvents are significantly lower than for water,[28] which is basically a reflection of the higher dipole density (low molecular weight) of water.

Literature Comparison. The existing relative permittivity data for both DMF and DMSO have been compiled recently by Wohlfarth.[29,30] However, many of the values listed by Wohlfarth are replicates, in that they are pure component data extracted from papers (from the same laboratory) reporting results for liquid mixtures. Some of the pure component ε_r values reported in these papers, mostly without comment, differ by as much as 2, which suggests they are of low accuracy. Unfortunately, the equations recommended by Wohlfarth[27] appear to have been fit to all of the data without weighting for uncertainty.

The available literature results for DMF are summarized in Table S1 in the Supporting Information and graphed in Figure 5. At $T = 298.15$ K and $p = 0.1$ MPa the reported ε_r values vary from 36.7 to 40.21, with values grouped around 39.4 ± 0.4 and 37.3 ± 0.6, the latter agreeing well with the present value of 37.26 ± 0.02. Probably fortuitously, the present $\varepsilon_r(T)$ values agree well (Figure 5) with the equation given by Wohlfarth.[27] Assuming no uncertainty for water impurity and

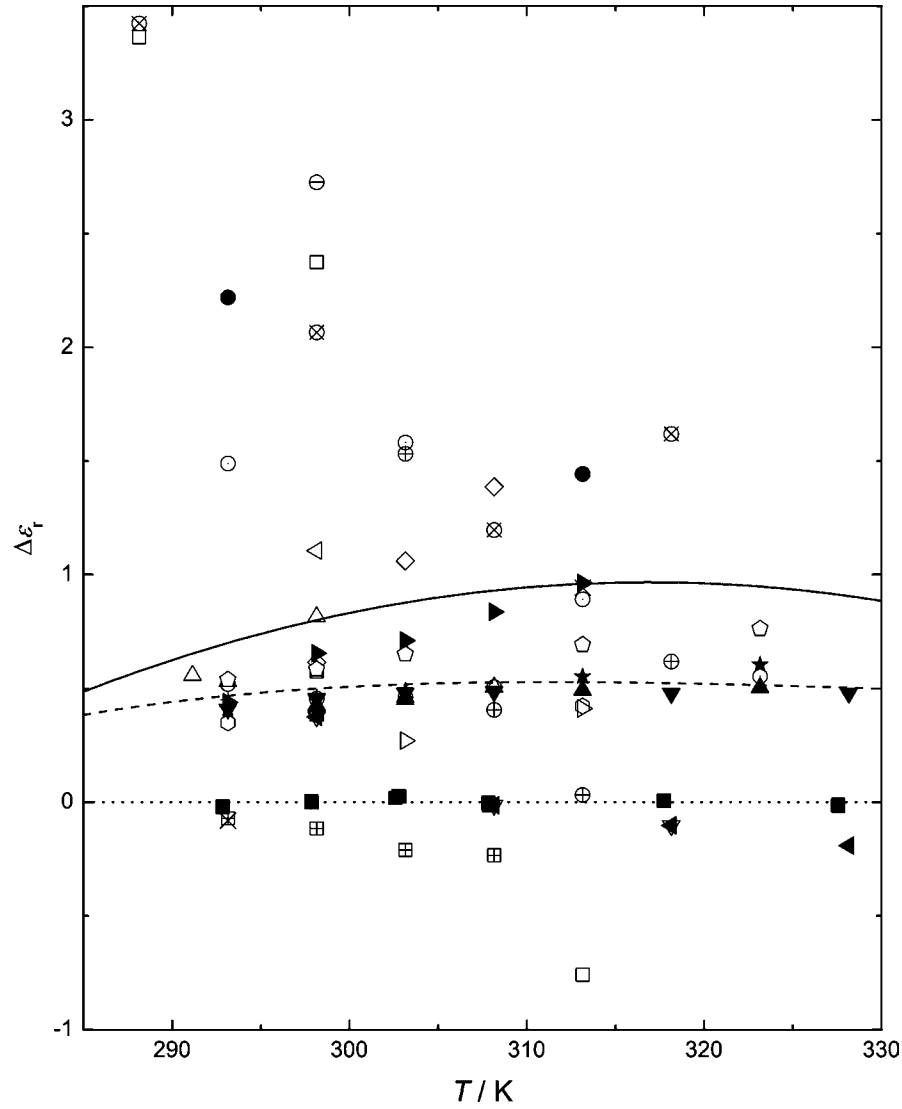

Figure 6. Absolute deviations, $\Delta\varepsilon_r = \varepsilon_{r,lit} - \varepsilon_r$, of literature data for DMSO at $p = 101.3$ kPa from permittivities, ε_r, calculated from eq 5 of this work obtained from mode 2: ■, measured values from this work; solid line represents $\varepsilon_r(T)$ recommended in ref 27; dashed line, recommended in ref 47; dotted line equals zero. For details of the literature data see Supporting Information.

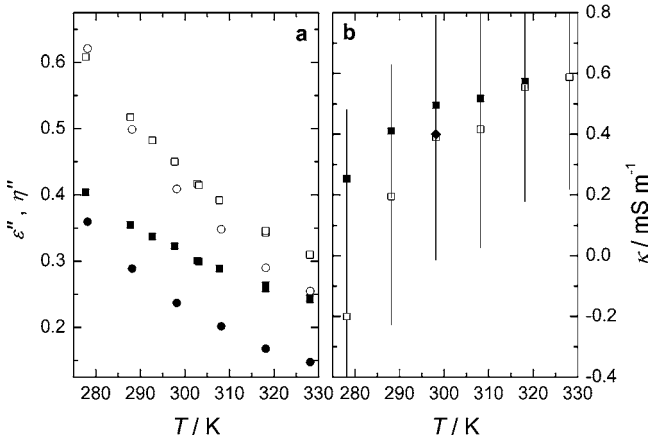

Figure 7. (a) Total loss, η'', for DMF, this work: ■, ≈ 110 MHz; □, ≈ 185 MHz. Dielectric loss, ε'', derived from ref 33: ●, ≈ 110 MHz; ○, ≈ 185 MHz. (b) Conductivity, κ, calculated from the difference $\eta'' - \varepsilon''(\kappa/2\pi f\varepsilon_0)$: ■, ≈ 110 MHz; □, ≈ 185 MHz; ♦, measured value. Vertical lines, estimated uncertainty.

values of ε_r in Table 1 adjusted to a constant temperature within 0.01 K gave a value of $(\partial\varepsilon_r/\partial p)_T = (28.6 \pm 1.0)$ TPa^{-1} for DMF that is virtually constant over the temperature range studied. Similarly, assuming no uncertainties for water impurities and 0.1 K temperature uncertainty, the temperature derivatives, $(\partial\varepsilon_r/\partial T)_p = (-0.177 \pm 0.006)$ K^{-1} and $(\partial^2\varepsilon_r/\partial T^2)_p = (11.5 \pm 0.1)\cdot 10^{-4}$ K^{-2} (both at $T = 298.15$ K), did not show a significant variation with pressure. This compares with literature values at 298.15 K of $(\partial\varepsilon_r/\partial T)_p = (-0.177$[27] and -0.170[47]) K^{-1} and $(\partial^2\varepsilon_r/\partial T^2)_p = (14.3$[27] and 9.7[47])$\cdot 10^{-4}$ K^{-2} both derived from the fit equations. The agreement is probably within the combined uncertainties.

Literature values for DMSO[30] are presented in Table S2 in the Supporting Information and plotted in Figure 6. There is considerable scatter in these data. Although most of the literature values are higher than the present results, there are five sets of data that agree with our ε_r values within our estimated uncertainty (see below) of 0.1. In particular, it should be noted that the greatest differences occur for the ε_r values determined by time domain spectroscopy, which have a high uncertainty. The differences between the present values and most of the literature data at $p = 0.1$ MPa are too large to be due to water contamination, even though the water content of the literature samples is often not stated, whereas that of the present sample is known to be low, $\{x(H_2O) \approx 0.002\}$. Further discussion of possible sources of this discrepancy is given in the following

section. As noted in the Introduction, Uosaki et al.[31] determined $\varepsilon_r(p)$ for DMSO at 298.15 K and p up to $p = 50$ MPa. A graphical representation of their data gives $(\partial\varepsilon_r/\partial p)_T = (12.3 \pm 0.3)$ TPa^{-1}. This value agrees with the present result of (12 ± 2) TPa^{-1} within our large experimental uncertainty (bearing in mind the limited pressure range of the present study). The value of $(\partial\varepsilon_r/\partial T)_p = (-0.131 \pm 0.002)$ K^{-1} for DMSO obtained at $p = 0.1$ MPa is considerably smaller than the corresponding value for DMF and was constant over the temperature and pressure range studied within the experimental uncertainties. Literature values at 298.15 K for $(\partial\varepsilon_r/\partial T)_p$ are (-0.113[27] and -0.126[47]) K^{-1} and $(\partial^2\varepsilon_r/\partial T^2)_p$ of (9.4[27] and 4.9[47]) $\cdot 10^{-4}$ K^{-2}. The last value in ref 47 is based on a critical selection of reliable values and is probably more accurate.

Sources of Uncertainty. The presence of air in the cavity would produce low permittivities, but the pressure test agreed well with the calculated compressibilities of the solvents; in addition, hysteresis would be expected within a pressure cycle. Since almost no hysteresis was observed, it is unlikely that the cavity was not filled completely. Uncertainties in the temperature of $\pm$ 0.1 K result in an uncertainty in ε_r of about $\pm$ 0.03.

The data analysis model makes a small contribution to the overall uncertainty.[9] Equation 3 is only valid for weak coupling to the external circuit; however, at the resonance frequency, $|S_{12}|$ was about 0.001, which is far from the critical value of 1, and thus, coupling effects were negligible. The model is also only accurate to first order in $1/Q$; for DMF and DMSO, terms of order $(1/Q)^2$ would amount to an uncertainty in ε_r of about 0.02. However, traditional methods like capacitor techniques also have to assume equivalent circuits, and the results so obtained may be biased by parasitic capacitances in the experimental setup especially if the solvent conductivity is high.

Another source of uncertainty is the possible dispersion of the permittivity at the relatively high measurement frequencies: $\approx$ (95 to 120) MHz for mode 2 and $\approx$ (165 to 200) MHz for mode 3. However, dielectric relaxation (DR) data for DMF[32] suggest that frequency dispersion should only produce differences from the static relative permittivity ranging from 0.001 to 0.004 at ambient pressure. Dispersion can, however, explain the difference between the values obtained from mode 2, ε_{r2}, and mode 3, ε_{r3}. Values of $\varepsilon_{r2} - \varepsilon_{r3}$ varying from 0.007 to 0.011 were observed, which are broadly consistent, given the uncertainties in both techniques, with the DR spectroscopic values of 0.0015 to 0.007 at temperatures from (278 to 328) K.

Sample impurities, primarily water, can be a source of uncertainty. For DMSO and DMF the addition of water leads to a higher relative permittivity as shown in several studies in the literature on the relative permittivity of binary DMSO + water[31,33,34] and DMF + water.[35] However, such effects will be very small ($\partial\varepsilon_r \approx 0.06$) on the basis of the measured water contents $\{x(H_2O) \approx 0.002\}$. In summary the estimated standard uncertainty at a 95 % confidence limit in ε_r accounting for all uncertainties including water content is estimated at 0.1.

The conductivity, κ, can be estimated at the frequencies studied by combining the measured $\hat{\eta}$ with DR estimates of the dielectric loss, ε''. For DMF Figure 7a shows that the difference $\eta'' - \varepsilon''$ is smaller for mode 3 than for mode 2. This is because the ohmic loss (conductivity) contribution scales with $1/f$. The uncertainty in η'' measured with the resonator is approximately 0.03 (equal to that of ε''), whereas the relative uncertainty of the DR ε'' values is $\approx$ 2 %. The conductivity calculated from the difference $\eta'' - \varepsilon''$ is shown in Figure 7b. Taking all sources of error into account, the uncertainties of the conductivities obtained are $2\cdot10^{-4}$ S·m^{-1} at 110 MHz and $4\cdot10^{-4}$ S·m^{-1} at 185 MHz. Thus, the deviation in the two conductivities determined using the two modes and the DR data is within the uncertainty of the determination and agrees with the experimental value. The deviation increases at lower temperatures, but this may be because κ is smaller at lower temperatures, causing the relative uncertainty to increase. For DMSO the DR spectrum is only available at 298 K,[36] but the slower dynamics of DMSO can explain the larger discrepancy between ε_{r2} and ε_{r3}, which ranges from 0.04 to 0.05 and also the higher absolute values of ε'' compared with DMF. The conductivity values obtained from mode 2 and mode 3, respectively, [$(2.2 \pm 1.1)\cdot10^{-4}$ and $(0.5 \pm 1.3)\cdot10^{-4}$] S·m^{-1}, are somewhat lower than the values measured at room temperature with a conductivity probe.

Kirkwood Correlation Factors. The Kirkwood−Fröhlich theory,[37,38] derived from statistical mechanics, can be used to gain insight into the molecular interactions in a single component dipolar liquid through the Kirkwood g factor obtained from:

$$g\mu^2 = \frac{9\varepsilon_0 k_B T M}{\rho N_A} \frac{(\varepsilon_r - \varepsilon_{r\infty})(2\varepsilon_r + \varepsilon_{r\infty})}{\varepsilon_r(\varepsilon_{r\infty} + 2)^2} \quad (6)$$

where k_B and N_A are the Boltzmann and Avogadro constants, respectively, M is the molar mass, ρ is the molar density, $\varepsilon_{r\infty}$ is the infinite frequency permittivity of the liquid, and μ is the dipole moment of the isolated molecule. For a random alignment of the molecular-level dipoles in a liquid $g = 1$, whereas values of $g < 1$ or $g > 1$ respectively indicate antiparallel and parallel statistical alignments. Kirkwood g factors thus yield indirect information on liquid structure. For the calculation of g as a function of temperature and pressure, density data $\rho(p,T)$ as well as $\varepsilon_{r\infty}$ values are required.

Table 5. Interpolated Relative Permittivity, ε_r, Obtained from Mode 2, Densities, ρ, Interpolated from Literature Data,[18−20] and Kirkwood Correlation Factors, g, Calculated According to Equation 6 for DMF and DMSO

T	ε_r		ρ/kg·dm^{-3}		g	
K	$p = 0.1$ MPa	$p = 5$ MPa	$p = 0.1$ MPa	$p = 5$ MPa	$p = 0.1$ MPa	$p = 5$ MPa
			DMF			
278.15	41.04	41.18	0.9628	0.9655	1.03	1.03
288.15	39.09	39.23	0.9535	0.9564	1.04	1.04
298.15	37.26	37.40	0.9441	0.9471	1.04	1.04
308.15	35.54	35.68	0.9346	0.9378	1.04	1.04
318.15	33.94	34.08	0.9250	0.9284	1.04	1.04
328.15	32.45	32.59	0.9153	0.9189	1.05	1.04
			DMSO			
293.15	46.68	46.72	1.0997	1.1023	1.02	1.01
298.15	46.02	46.07	1.0954	1.0980	1.03	1.02
308.15	44.71	44.77	1.0866	1.0893	1.05	1.04
318.15	43.40	43.46	1.0779	1.0807	1.06	1.06
328.15	42.09	42.16	1.0691	1.0720	1.08	1.07

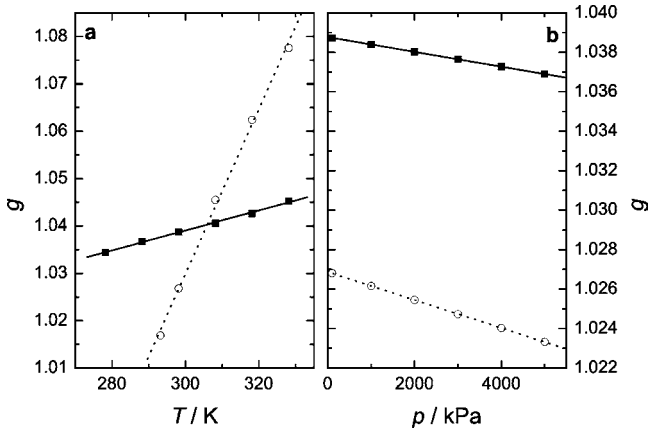

Figure 8. Kirkwood correlation factors g calculated from eq 6 at (a) p = 0.1 MPa: ■, DMF; ○, DMSO. (b) T = 298.15 K: ■, DMF; ○, DMSO. Lines are for visual aid.

The various $\rho(p,T)$ data sets available for DMF[19,20] at 288.15 ≤ T/K ≤ 313.15 were combined and interpolated or extrapolated to give the densities listed in Table 5. For DMSO $\rho(p,T)$ was taken from ref 18. For both DMF and DMSO, $\varepsilon_{r\infty}$ was approximated as $1.1n^2$ where n is the refractive index of the liquid at the sodium D line.[39] The multiplicative factor of 1.1 accounts approximately for vibrational modes not excited by the Na D line. Values of $n(p,T)$ were calculated from the Lorentz−Lorenz[40] equation:

$$[R] = \frac{n^2 - 1}{n^2 + 2}\frac{M}{\rho N_A} \qquad (7)$$

assuming a constant molar refraction, $[R]$, of 19.97 $cm^3 \cdot mol^{-1}$ for DMF and 20.23 $cm^3 \cdot mol^{-1}$ for DMSO.[41] The dipole moments of DMF and DMSO were taken as $\mu = 12.7 \cdot 10^{-30}$ C·m and $\mu = 13.2 \cdot 10^{-30}$ C·m, respectively.[27]

The calculated correlation factors are summarized in Table 5. For both liquids the present correlation factors agree well with the values obtained with other experimental techniques[32,42−44] and molecular dynamic simulations.[45] At all temperatures and pressures g values are slightly higher than unity, suggesting a marginal preference for parallel alignment of the molecular dipoles in both solvents. The effects of temperature (at p = 0.1 MPa) and pressure (at T = 298.15 K) on the correlation factor are plotted in Figure 8. The present data indicate that g increases with increasing temperature and decreasing pressure, which yields a small negative activation energy for the dipole−dipole interaction. However, the variation of g with T and p is very small (Table 5), so these trends may well be just a reflection of the uncertainties in $\varepsilon_{r\infty}$ and ρ. In particular, $\varepsilon_{r\infty}$ could be greater than $1.1n^2$ because of atomic polarization and the neglect of effects due to inter- and intramolecular vibrations (it is known that DMF exhibits a high frequency mode at ≈ 160 GHz[32]).

Conclusions

The relative permittivity of DMF measured with a re-entrant radio frequency resonator at p = 0.1 MPa agreed with reliable literature values. A value of $(\partial\varepsilon_r/\partial p)_T = (28.6 \pm 1.0)$ TPa^{-1} was obtained for DMF from measurements at $p \le 5$ MPa. For DMSO the measured ε_r was lower than most literature values, while $(\partial\varepsilon_r/\partial p)_T$ agreed within an extrapolated value with the combined uncertainties. For both solvents the Kirkwood g factor was slightly higher than 1, indicating a slight tendency for parallel alignment of the dipoles.

Radio-frequency and microwave resonant cavities are probably the most precise technique currently available for measuring $\varepsilon_r(p,T)$ of fluids of conductance of $\lesssim 1 \cdot 10^{-2}$ $S \cdot m^{-1}$. The present cavity is limited in both its temperature and pressure range, so results were not as precise as expected. Ideally, for measurements of $\varepsilon_r(p,T)$ a cavity should be usable at pressures up to at least 100 MPa and be capable of operating over a 200 K temperature range. It should have at least two modes with vacuum frequencies sufficiently high so that the instrumentation can cope with the addition of a high permittivity fluid. The need to minimize high purity sample consumption will influence the design.

Supporting Information Available:

Literature data on the permittivity of DMF and DMSO and comparison with the present data in both tabular and graphical form. This material is available free of charge via the Internet at http://pubs.acs.org.

Literature Cited

(1) Drude, P.; Nernst, W. On the electrostriction induced by free ions. *Z. Phys. Chem. (München, Ger.)* **1894**, *15*, 79–85.
(2) Brouillette, D.; Perron, G.; Desnoyers, J. E. Apparent molar volume, heat capacity, and conductance of lithium bis(trifluoromethylsulfone)imide in glymes and other aprotic solvents. *J. Solution Chem.* **1998**, *27*, 151–182.
(3) Marcus, Y.; Hefter, G. On the pressure and electric field dependencies of the relative permittivity of liquids. *J. Solution Chem.* **1999**, *28*, 575–592.
(4) Chadwick, S. S. *Ullmann's Encyclopedia of Industrial Chemistry*; Wiley-VCH: Weinheim, 2006.
(5) Moldover, M. R.; Marsh, K. N.; Barthel, J.; Buchner, R. Relative permittivity and refractive index. In *Experimental Thermodynamics*; Goodwin, A. R. H., Marsh, K. N., Wakeham, W. A., Eds.; Elsevier: Amsterdam, 2003; Vol. VI.
(6) Goodwin, A. R. H.; Mehl, J. B.; Moldover, M. R. Reentrant radio-frequency resonator for automated phase-equilibria and dielectric measurements in fluids. *Rev. Sci. Instrum.* **1996**, *67*, 4294–4303.
(7) Kandil, M. E.; Marsh, K. N.; Goodwin, A. R. H. Determination of the relative permittivity and density within the gas phase and liquid volume fraction formed within the two-phase region for (0.4026 CH_4 + 0.5974 C_3H_8) with a radio frequency re-entrant cavity. *J. Chem. Eng. Data* **2007**, *52*, 1660–1671.
(8) May, E. F.; Edwards, T. J.; Mann, T. J.; Edwards, C. Dew point, liquid volumes and dielectric constant measurements in a vapor mixture of methane + propane using a microwave apparatus. *Int. J. Thermophys.* **2003**, *24*, 1509–1525.
(9) May, E. F.; Edwards, T. J.; Mann, T. J.; Edwards, C.; Miller, R. C. Development of an automated phase behaviour measurement system for lean hydrocarbon fluid mixtures, using re-entrant rf/microwave resonant cavities. *Fluid Phase Equilib.* **2001**, *185*, 339–347.
(10) May, E. F.; Edwards, T. J.; Mann, T. J.; Edwards, C. An improved microwave apparatus for phase behaviour measurements in lean gas condensate fluids. *Fluid Phase Equilib.* **2004**, *215*, 245–252.
(11) May, E. F.; Miller, R. C.; Goodwin, A. R. H. Dielectric constants and molar polarizabilities for vapor mixtures of methane + propane, and methane + propane + hexane obtained with a radio frequency reentrant cavity. *J. Chem. Eng. Data* **2002**, *47*, 102–105.
(12) Kandil, M. E.; Marsh, K. N.; Goodwin, A. R. H. Determination of the relative permittivity, ε', of methylbenzene at temperatures between (290 and 406) K, and pressures below 20 MPa with a radio frequency re-entrant cavity and evaluation of a MEMS capacitor for the measurement of ε'. *J. Chem. Eng. Data* **2008**, *53*, 1056–1065.
(13) Goodwin, A. R. H.; Mehl, J. B. Measurement of the dipole moments of seven partially fluorinated hydrocarbons with a radiofrequency reentrant cavity resonator. *Int. J. Thermophys.* **1997**, *18*, 795–806.
(14) Hamelin, J.; Mehl, J. B.; Moldover, M. R. The static dielectric constant of liquid water between 274 and 418 K near the saturated vapor pressure. *Int. J. Thermophys.* **1998**, *19*, 1359–1380.
(15) Hamelin, J.; Mehl, J. B.; Moldover, M. R. Resonators for accurate dielectric measurements in conducting liquids. *Rev. Sci. Instrum.* **1998**, *69*, 255–260.
(16) Anderson, G. S.; Miller, R. C.; Goodwin, A. R. H. Static dielectric constants for liquid water from 300 to 350 K at pressures to 13 MPa using a new radio-frequency resonator. *J. Chem. Eng. Data* **2000**, *45*, 549–554.

(17) http://physics.nist.gov/cuu/Constants/index.html (accessed Jan 26, 2010).
(18) Petitet, J. P.; Bezot, P.; Hesse-Bezot, C. Thermodynamic properties of (0.32 DMSO-H_2O) mixture and pure DMSO under pressure. *Physica B (Amsterdam, Neth.)* **1988**, *153*, 181–190.
(19) García-Giménez, P.; Martínez-López, J. F.; Blanco, S. T.; Velasco, I.; Otín, S. Densities and isothermal compressibilities at pressures up to 20 MPa of the systems *N*,*N*-dimethylformamide or *N*,*N*-dimethylacetamide + α,ω-dichloroalkane. *J. Chem. Eng. Data* **2007**, *52*, 2368–2374.
(20) Zúñiga-Moreno, A.; Galicia-Luna, L. A. Compressed liquid densities and excess volumes for the binary system CO_2 + *N*,*N*-dimethylformamide (DMF) from (313 to 363) K and pressures up to 25 MPa. *J. Chem. Eng. Data* **2005**, *50*, 1224–1233.
(21) http://www.kayelaby.npl.co.uk/general_physics/2_6/2_6_1.html (accessed Jan 26, 2010).
(22) Schmidt, J. W.; Gavioso, R. M.; May, E. F.; Moldover, M. R. Polarizability of helium and gas metrology. *Phys. Rev. Lett.* **2007**, *98*, 254504.
(23) McCarty, R. D.; Arp, V. D. A new wide range equation of state for helium. *Adv. Cryog. Eng.* **1990**, *35*, 1465–1475.
(24) Harvey, A. H.; Lemmon, E. W. Method for estimating the dielectric constant of natural gas mixtures. *Int. J. Thermophys.* **2005**, *26*, 31–46.
(25) Lemmon, E. W.; McLinden, M. O.; Huber, M. L. *Reference fluid thermodynamic and transport properties*, NIST Standard Reference Database 23, Version 8.0; NIST: Gaithersburg, MD, 2007.
(26) Bauccio, M. *ASM Metals Reference Book*; ASM International: Akron, OH, 1993.
(27) *CRC-Handbook of Chemistry and Physics*, 85th ed.; Lide, D. R., Ed.; CRC Press: Boca Raton, FL, 2004.
(28) Fernandez, D. P.; Goodwin, A. R. H.; Lemmon, E. W.; Levelt Sengers, J. M. H.; Williams, R. C. A Formulation for the static permittivity of water and steam at temperatures from 238 to 873 K at pressures up to 1200 MPa, including derivatives and Debye-Hückel coefficients. *J. Phys. Chem. Ref. Data* **1997**, *26*, 1125–1166.
(29) Wohlfarth, C. Dielectric constant of *N*,*N*-dimethylformamide. In *Landolt-Börnstein: Numerical Data and Functional Relationships in Science and Technology - New Series: Static Dielectric Constants of Pure Liquids and Binary Liquid Mixtures*; Madelung, O., Ed.; Springer: Berlin, 2008; Vol. 17, pp 175−182.
(30) Wohlfarth, C. Dielectric constant of dimethylsulfoxide. In *Landolt-Börnstein: Numerical Data and Functional Relationships in Science and Technology - New Series: Static Dielectric Constants of Pure Liquids and Binary Liquid Mixtures*; Madelung, O., Ed.; Springer: Berlin, 2008; Vol. 17, pp 140−143.
(31) Uosaki, Y.; Kitaura, S.; Moriyoshi, T. Static relative permittivities of water + acetone and water + dimethyl sulfoxide under pressures up to 300 MPa at 298.15 K. *J. Chem. Eng. Data* **1997**, *42*, 580–584.
(32) Barthel, J.; Buchner, R.; Wurm, B. The dynamics of liquid formamide, *N*-methylformamide, *N*,*N*-dimethylformamide, and *N*,*N*-dimethylacetamide. A dielectric relaxation study. *J. Mol. Liq.* **2002**, *98*, 51–69.
(33) Kaatze, U.; Pottel, R.; Schäfer, M. Dielectric spectrum of dimethyl sulfoxide/water mixtures as a function of composition. *J. Phys. Chem.* **1989**, *93*, 5623–5627.
(34) Puranik, S. M.; Kumbharkhane, A. C.; Mehrotra, S. C. Dielectric study of dimethyl sulfoxide-water mixtures using the time-domain technique. *J. Chem. Soc., Faraday Trans.* **1992**, *88*, 433–435.
(35) Cooke, C.; McCallum, C.; Pethybridge, A. D.; Prue, J. E. Conductance of acids in dimethylsulphoxide-I: Conductance of hydrochloric acid in DMSO−water mixtures at 25 °C. *Electrochim. Acta* **1975**, *20*, 591–598. (a) Kim, J. I.; Cecal, A.; Born, H. J.; Gomaa, E. A. Preferential solvation of single ions: A critical study of the Ph_4AsBPh_4 assumption for single ion thermodynamics in mixed aqueous-acetonitrile and aqueous-*N*,*N*-dimethylformamide solvents. *Z. Phys. Chem. (München, Ger.)* **1978**, *110*, 209–227.
(36) Barthel, J.; Bachhuber, K.; Buchner, R.; Gill, J. B.; Kleebauer, M. Dielectric spectra of some common solvents in the microwave region. Dipolar aprotic solvents and amides. *Chem. Phys. Lett.* **1990**, *167*, 62–66.
(37) Fröhlich, H. *Theory of Dielectrics*, 2nd ed.; Oxford University Press: Oxford, 1965.
(38) Kirkwood, J. G. The dielectric polarization of polar liquids. *J. Chem. Phys.* **1939**, *7*, 911–919.
(39) Stokes, R. H.; Marsh, K. N. A stepwise dilution technique for measuring the static dielectric properties of liquid mixtures. Dielectric behavior of ethanol in cyclohexane, *n*-hexane, carbon tetrachloride, benzene, *p*-xylene, and carbon disulphide. *J. Chem. Thermodyn.* **1976**, *8*, 709–723.
(40) Böttcher, C. F. J. *Theory of Electrical Polarization*; Ed.; Elsevier: Amsterdam, 1973, Vol. 1, and 1978, Vol. 2 (with Bordewijk, P.).
(41) Pacak, P. Polarizability and molecular radius of dimethyl-sulfoxide and dimethylformamide from refractive index data. *J. Solution Chem.* **1987**, *16*, 71–77.
(42) Bass, S. J.; Nathan, W. I.; Meighan, R. M.; Cole, R. H. Dielectric properties of alkyl amides. II. Liquid dielectric constant and loss. *J. Phys. Chem.* **1964**, *68*, 509–515.
(43) Kinart, M. C.; Bald, A.; Kinart, W. J.; Kolasinski, A. Dimethylsulfoxide-*N*,*N*-dimethylformamide binary mixtures and their physicochemical properties. *Phys. Chem. Liq.* **1998**, *36*, 245–256.
(44) Prestbo, E. W.; McHale, J. L. Static dielectric constants and Kirkwood correlation factors of dimethyl sulfoxide/carbon tetrachloride solutions. *J. Chem. Eng. Data* **1984**, *29*, 387–389.
(45) Richardi, J.; Krienke, H.; Fries, P. H. Dielectric constants of liquid formamide, *N*-methylformamide and dimethylformamide via molecular Ornstein-Zernike theory. *Chem. Phys. Lett.* **1997**, *273*, 115–121.
(46) Barthel, J.; Neueder, R. Conductivities, transference numbers, and limiting ionic conductivities of protophilic H-bond donor and aprotic solvents. I: Amides. In *Electrolyte Data Collection* (Part 1g); Kreysa, G., Ed.; DECHEMA: Frankfurt, 2001; Vol. XII.
(47) Barthel, J.; Neueder, R. Conductivities, transference numbers, and limiting ionic conductivities of protophilic H-bond donor and aprotic solvents. II: Aprotic solvents, except amides. In *Electrolyte Data Collection* (Part 1h); Kreysa, G., Ed.; DECHEMA: Frankfurt, 2003; Vol. XII.

Received for review December 22, 2009. Accepted January 11, 2010. K.M. acknowledges the award of a Gledden Fellowship by the University of Western Australia. J.H.'s time in Perth was funded by Murdoch University.

JE9010773